Pergamon

PII:S0899-5362(00)00059-2

Journal of African Earth Sciences, Vol. 30, No. 4, pp. 903–916, 2000

0899-5362/00 $- see front matter

Mapping gossans in arid regions with Landsat TM and SIR-C images: the Beddaho Alteration Zone in northern Eritrea

MOHAMED G. ABDELSALAM[1,*], ROBERT J. STERN[1]
and WOLDEGABRIEL G. BERHANE[2]
[1]Center for Lithospheric Studies, The University of Texas at Dallas,
Richardson, TX, 75083-0688, USA
[2]Department of Mines, The Geological Survey, Asmara, Eritrea

ABSTRACT—Massive sulphide deposits in the Neoproterozoic Arabian-Nubian Shield are exposed at the surface as Fe-rich crusts termed gossans. Gossans are typically a few tens of metres across but are surrounded by wider clay- and Fe-rich alteration zones. Although Fe-rich gossans have characteristic reflectance spectra and surface roughness, they are often too small to be directly detected by Landsat TM or SIR-C images, both of which have about 30 m spatial resolution. In this paper, a procedure is described whereby gossans and the surrounding alteration zones can be identified and mapped by Landsat TM and SIR-C data using the Beddaho Alteration Zone and the Tebih Gossan in northern Eritrea as an example. Clay and Fe alteration index maps were generated by density slicing for Landsat TM band-ratios 5/7 and 3/1, respectively. Landsat 5/7-4/5-3/1 TM images characteristically depict small (tens of pixels) gossans in blue and the more extensive alteration zones in pinkish purple. Chh-Lhh-Lhh/Chh SIR-C images succeeded in identifying the gossan due to enhanced back-scattering of the radar shorter wavelength (6 cm) C-band by the rough gossan surfaces. This enhanced back-scattering might also be partially due to the characteristic dielectric property of the Fe-rich minerals forming the gossans. Choosing known gossans from both 5/7-4/5-3/1 Landsat TM and Chh-Lhh-Lhh/Chh SIR-C images as training sites for supervised classification helped to outline areas with reflectance spectra and radar back-scattering properties similar to those of the training sites. These results show significant correlation between supervised classifications based on the two data sets, suggesting a way to use combined visible and near infrared (VNIR) and radar imagery to explore for mineral deposits in arid regions.

RÉSUMÉ—Les amas sulfurés massifs du Bouclier néoprotérozoïque arabo-nubien affleurent à la surface sous forme de croûtes riches en fer appelées 'gossans'. Les gossans ont typiquement une extension de quelques dizaines de mètres et sont entourés par des zones d'altération plus larges à argiles et riches en Fe. Bien que les gossans riches en Fe présentent un spectre de réflectance et une rugosité de surface caractéristiques, ils sont souvent trop petits pour être détectés directement sur les images Landsat TM ou SIR-C, dont la résolution spatiale est d'environ 30 m. Cet article décrit une procédure permettant d'identifier et de cartographier à partir des données Landsat TM et SIR-C les gossans et les zones périphériques d'altération, en prenant pour exemple la zone d'altération de Beddaho et le gossan de Tebih en Erythrée du nord. Les cartes d'indice d'altération en argiles et en Fe ont été dressées par tranches d'isodensité des rapports de bandes Landsat TM 5/7 et 3/1, respectivement. Les images Landsat 5/7-4/5-3/1 TM représentent de façon caractéristique de petits gossans (dizaines de pixels) en bleu et les zones d'altération plus larges en pourpre rosé. Les images Chh-Lhh-Lhh/Chh SIR-C ont réussi à identifier le gossan à cause de l'accroissement de la rétro-diffusion de la bande C de

*Corresponding author
abdels@utdallas.edu

la plus courte longueur d'onde radar (6 cm) par les surfaces rugueuses du gossan. L'accroissement de la rétro-diffusion a pu être due partiellement à la propriété diélectrique caractéristique des minéraux riches en Fe qui forment le gossan. Le choix de gossans connus comme sites de vérification pour une classification revue à partir des images 5/7-4/5-3/1 Landsat TM et Chh-Lhh-Lhh/Chh SIR-C a aidé à définir les zones dont les spectres de réflectance et les propriétés de rétro-diffusion radar sont semblables aux sites de vérification. Ces résultats montrent une corrélation significative entre les classifications revues fondues sur les deux groupes de données, suggérant une méthode d'utilisation combinée de l'imagerie visible et proche-infra rouge (VNIR) et radar pour l'exploration de gîtes minéraux en zones arides.

(Received 24/12/99: revised version received 3/5/00: accepted 3/5/00)

INTRODUCTION

Gold deposits and the geology of the Arabian-Nubian Shield have long been an important association and promises to continue to be important. Gold has been extracted from northeast Africa for more than 5000 years (Hume, 1937), and this may be the first place where this metal was extracted by humans. Indeed, the word 'Nubia' comes from the ancient Egyptian word for gold – Nub. The hosts for these Au deposits are Neoproterozoic rocks of the Arabian-Nubian Shield (Fig. 1). The Arabian-Nubian Shield consists of juvenile continental crust that formed between 900 and 550 Ma, when intra-oceanic arc terranes welded together along ophiolite-decorated arc-arc sutures (Stern, 1994; Abdelsalam and Stern, 1996a). Primary Au mineralisation probably developed in association with the growth of intra-oceanic arcs and evolution of back-arc basins. Multiple episodes of deformation, metamorphism and intrusion have obscured the primary metallogenetic setting, but at least some of the deposits preserve evidence that they originated as seafloor massive sulphide deposits.

The Neoproterozoic basement on both sides of the Red Sea host auriferous massive sulphide ore bodies (Al-Shanti and Roobol, 1979). These massive sulphides are broadly Kuroko-type and formed by submarine hydrothermal activity associated with felsic intrusions. Primary mineralisation occurs as both stock-work and stratabound deposits, which were then faulted, folded, metamorphosed and intruded. Recent interaction with air and surface water oxidised the sulphides, yielding Fe-rich crusts termed gossans (Sato, 1974). Pyrite plus water produces insoluble Fe oxides and sulphuric acid with the result that the near-surface portions of a sulphide ore body will be oxidised and many soluble elements reconcentrated in the gossan or leached away (Kearey, 1993).

Excellent examples of auriferous massive sulphide deposits in the Arabian-Nubian Shield occur in the Ariab Metallogenic District of the Red Sea Hills of the Sudan (Aye *et al.*, 1985; Cottard *et al.*, 1986; Bakheit and Matheis, 1993; Wipfler, 1994), and the Mahd adh Dahhab (Arabic for 'the cradle of gold') deposit in Saudi Arabia (Goldsmith and Kouther, 1971). Both deposits occur in polydeformed and metamorphosed volcano-sedimentary rocks of the Neoproterozoic Nakasib-Bir Umq Suture (Johnson, 1994). The Mahd adh Dahhab deposit contains quartz veins with visible Au and thus was known from ancient times, whereas the Ariab deposits contains invisible Au and so was not discovered until 1984. Other massive sulphide deposits have been described from the southern Arabian Shield (Ryall and Taylor, 1981). Discovery of other 'invisible gold' deposits can be expected elsewhere in the vast and poorly known Arabian-Nubian Shield. Efficient exploration for these deposits will naturally focus on first finding gossans and associated alteration zones, a task that is well suited for modern remote sensing techniques.

This work describes the use of Landsat thematic mapper (TM) and shuttle imaging radar (SIR)-C data to map gossans in arid regions using the Beddaho Alteration Zone in northern Eritrea (Fig. 1) as an example. The Beddaho Alteration Zone has well-developed gossans surrounded by a wider zone of clay- and Fe-rich alteration. Although these gossans have characteristic reflectance spectra, they are often smaller (few tens of metres across) than the 28.5 m pixel size of Landsat TM images. Moreover, in spite of the fact that gossans have rougher surfaces than the surrounding volcano-sedimentary and plutonic rocks, their small size makes it difficult to find them with SIR-C images where spatial resolution is 30 m. The procedure outlined below made it possible to use relatively poor spatial resolution Landsat TM data to locate gossans. This is followed by interpretation of the SIR-C images over the mineralised area to evaluate the potential of orbital imaging radar as a mineral exploration tool.

REGIONAL SETTING

The Neoproterozoic basement of northern Eritrea (Fig. 1) lies in the central part of the East African Orogen, just north of the transition between the Arabian-Nubian Shield and the Mozambique Belt (Stern, 1994). The East African Orogen contains intra-oceanic arc

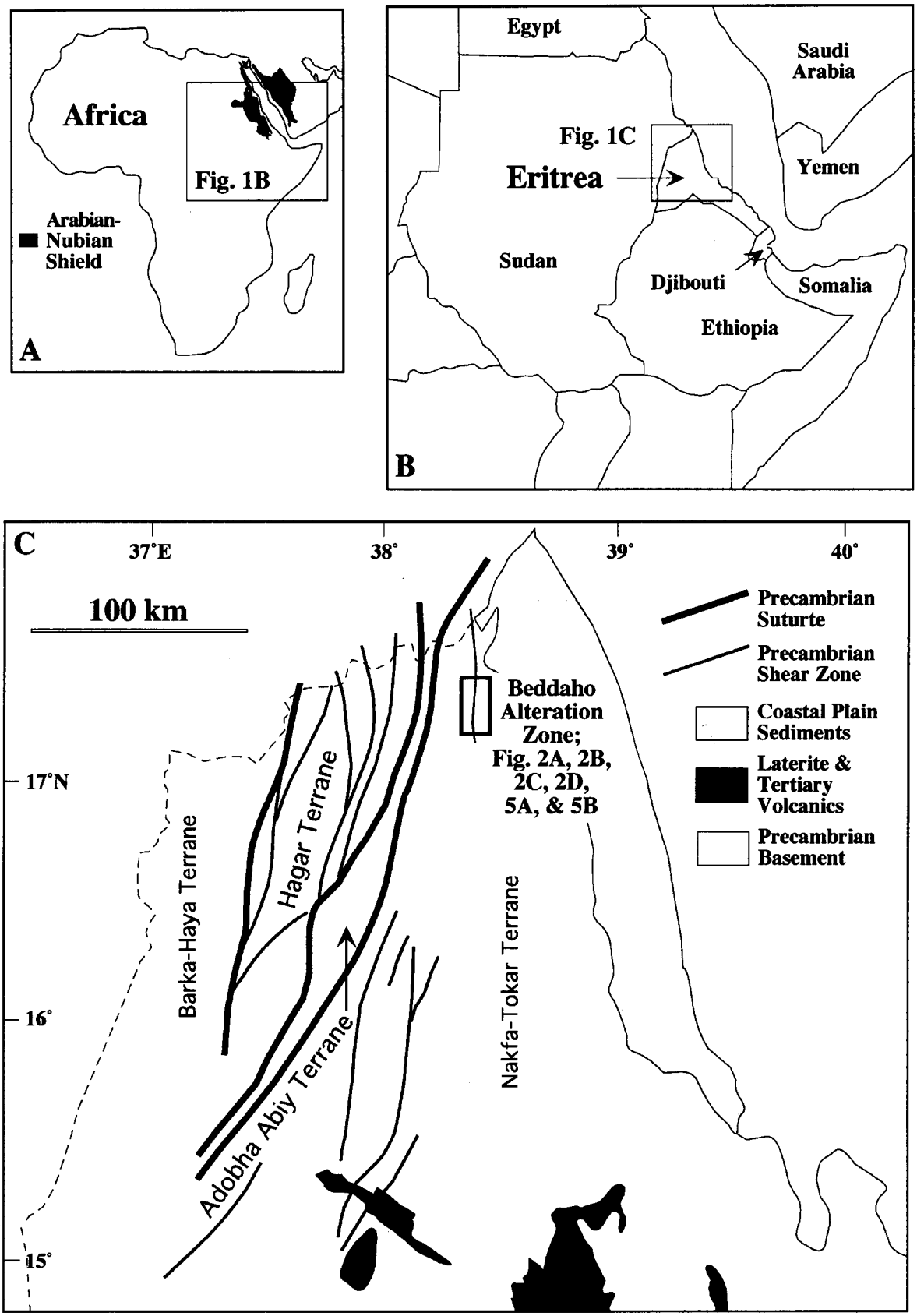

Figure 1. *Locality map of the study area. (A) Africa. (B) Northeast Africa. (C) Structural map of Eritrea (after Drury* et al., *1994; Drury and de Souza Filho, 1999).*

terranes welded along arc-arc sutures sandwiched between continental fragments of east and west Gondwana as they collided in the late Neoproterozoic along arc-continent or continent-continent sutures.

The Neoproterozoic structures in Eritrea (Fig. 1) are mainly upright folds, thrust faults, shear zones and strike-slip faults, all of which trend approximately north-south (Drury and Berhe, 1993; de Souza Filho and Drury, 1998; Drury and de Souza Filho, 1999). This geometry and style of deformation is similar to the Mozambique Belt further south (Shackleton, 1986; Key *et al.*, 1989; Mosely, 1993) and to the Asir Terrane of Arabia (Stoeser and Camp, 1985) and post-accretionary shear zones in Sudan to the north (Miller and Dixon, 1992; Abdelsalam, 1994). Neoproterozoic deformation of the Eritrean basement records collision and sinistral shearing of at least four terranes along north-northeast and north-northwest-trending sutures (Fig. 1)(Drury and Berhe, 1993; Teklay, 1997; Beyth *et al.*, 1997; de Souza Filho and Drury, 1998; Drury and de Souza Filho, 1999). The westernmost Barka-Haya Terrane is dominated by multiply deformed gneisses and evolved silicic volcanic rocks. The Hagar Terrane is dominated by immature arc volcanics and ophiolite fragments. The Adobha Abiy Terrane is dominated by sediments. Farther east, the Nakfa-Tokar Terrane occupies more than half of the Neoproterozoic basement of Eritrea and is composed of volcano-sedimentary rocks, dismembered ophiolites, quartzo-feldspathic gneiss and syn-tectonic granitoids.

The Beddaho Alteration Zone (Fig. 1) occurs in the Nakfa-Tokar Terrane, which yields radiometric ages of ~630 to ~850 Ma (Kröner *et al.*, 1991; Teklay, 1997). This part of the Nakfa-Tokar Terrane is dominated by a volcano-sedimentary sequence sheared against quartzo-feldspathic gneiss. Syn-tectonic granodioritic bodies intrude both lithological units (Fig. 2). Primary mineralisation in the Beddaho Alteration Zone probably occurred about the time that the volcano-sedimentary sequence was being deposited, about 850 Ma (Teklay, 1997). The terrain around the deposit is rugged, with a relief of about 750 m, corresponding to ~650 m elevation on the wadi floors to ~1400 m on summits.

GEOLOGY AND ORBITAL IMAGES OF THE BEDDAHO ALTERATION ZONE

No geological map has been published for the region around the Beddaho Alteration Zone. Phelps Dodge mining company has studied the deposit (Toogood, *pers. comm.*). In this study, Landsat TM and SIR-C images were used together with observations from two weeks of fieldwork to map lithological units and structures within and around the Beddaho Alteration Zone (Fig. 2). The characteristics of the orbital remote sensing data will be discussed later. The following discussion refers to false-colour Landsat TM and SIR-C images (Fig. 2A, B, C) produced from three components assigned to the colours red, green and blue (RGB), in that order (Fig. 2D). The authors started with a 7-4-2 Landsat TM image (Fig. 2A) recommended for geological studies in arid regions by Sabins (1997). In the study area, lithological units and the alteration zone are poorly defined in this image. Because Neoproterozoic structures in this region are defined by the distribution of lithologies, basement structures are also poorly resolved in this image. The 5/7-4/5-3/1 Landsat TM band-ratio image produced by dividing digital numbers (DN) of one band by another to yield an image that enhances spectral differences and reduces topographic variation in illumination. This image better reveals lithological variations and the Neoproterozoic structures. The alteration zone is outlined well in this image, where it appears pink with tinges of purple (Fig. 2B). Landsat TM band-ratios 5/7 and 3/1 emphasises clay and Fe minerals that have specific spectral reflectance and absorption features in these bands, respectively (Sabins, 1997), as will be discussed later. Band-ratio 4/5 is used because hydroxyl minerals have reflectance maxima at band 4 and absorption minima at band 5 (Abrams *et al.*, 1983; Ruiz-Armenta and Prol-Ledesma, 1998).

Due to the roughness of the terrain, the Chh-Lhh-Lhh/Chh SIR-C image (Fig. 2C) is not useful for detecting large-scale lithological variations. From now on this will be referred to as the shuttle radar image. In this image, C band (wavelength = 6 cm) with polarisation hh (horizontally transmitted and horizontally received) is assigned to the colour red, L band (wavelength = 24 cm) with polarisation hh is assigned to green, and the band-ratio Lhh/Chh is assigned to blue. This combination has been shown to be useful for other types of geological studies in arid regions (Abdelsalam and Stern, 1996b). Chh-Lhh-Lhh/Chh SIR-C images are useful for mapping young faults related to the Red Sea rifting as discussed by Drury *et al.* (1994) because of the better morphological expression of these faults (Abdelsalam *et al.*, 2000).

Landsat TM and SIR-C images, together with field checking, allowed us to effectively map an area of about 450 km^2 (Fig. 2E). In addition to the Beddaho Alteration Zone, four broad lithological units were identified: quartzo-feldspathic gneiss, volcano-sedimentary rocks, syn-tectonic granitoids and post-tectonic granitoids.

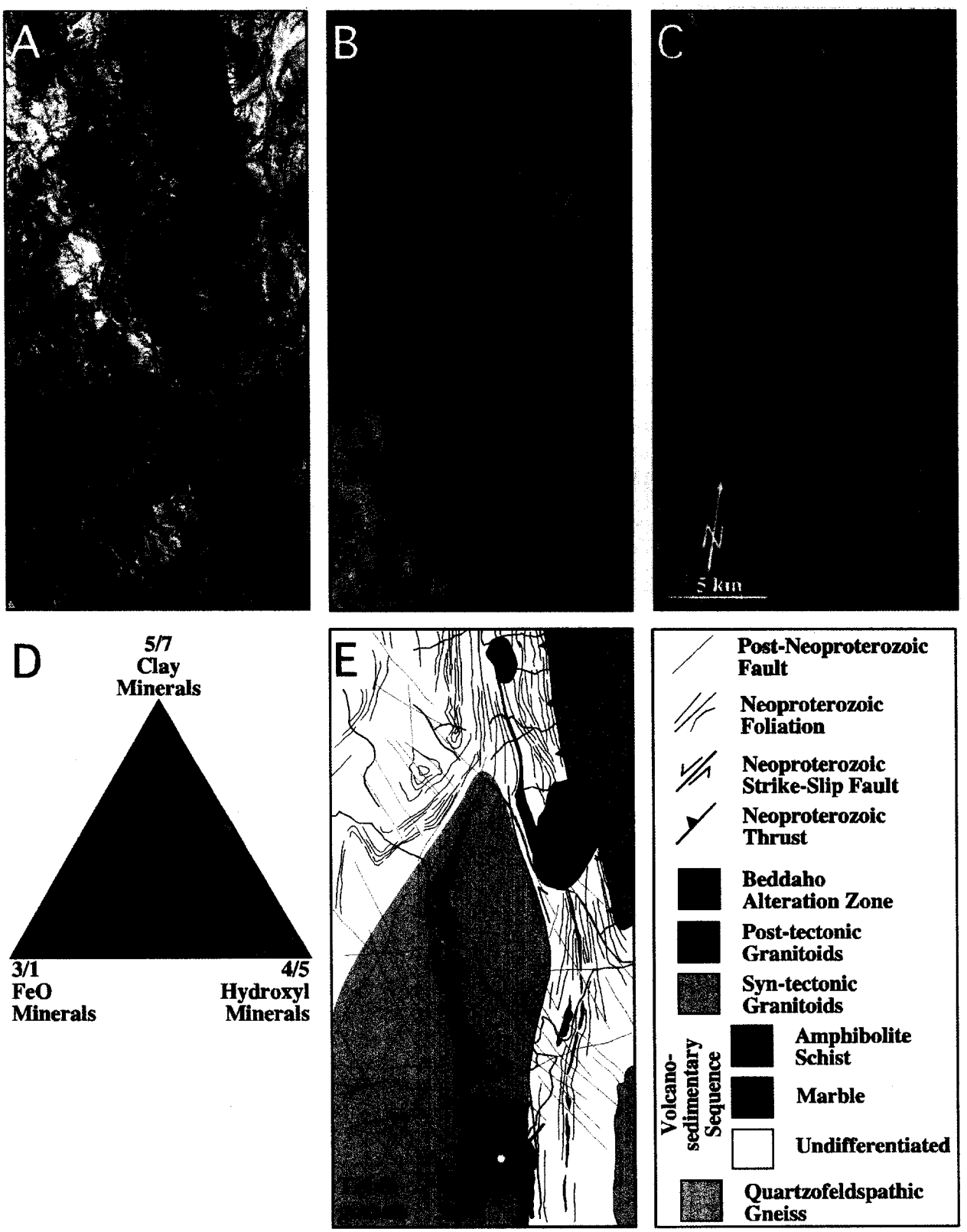

Figure 2. *Remote sensing images and geological map of the Beddaho Alteration Zone. (A) 7-4-2 Landsat TM image. (B) 5/7-4/5-3/1 Landsat TM image. (C) Chh-Lhh-Lhh/Chh SIR-C image. Radar illumination is to the southeast. (D) RGB colour overlay triangle showing the relationships between Landsat TM band-ratios 5/7 (red), 4/5 (green), and 3/1 (blue) and the end-member clay, FeO, and hydroxyl minerals, respectively. (E) Geological map.*

The quartzo-feldspathic gneiss occupies the northeastern part of the map area (Fig. 2E). The gneiss is dominantly pale pink and is made up of quartz, K-feldspar, plagioclase, biotite and hornblende with rare garnet porphyroblasts. Gneissic layering is defined by ~ 1 cm wide leucosomes dominated by quartz and feldspars and melanosomes where biotite and brown hornblende are as important as quartz and feldspar. The gneiss outcrops in low-lying hills that continue eastward until it is buried beneath the Red Sea coastal plain.

The gneiss domain appears white in the 7-4-2 Landsat TM image (Fig. 2A) and pale pinkish-blue in the 5/7-4/5-3/1 Landsat TM image (Fig. 2B). None of these images reveals the well-developed mesoscopic north-trending planar fabric of the gneiss. This is due to the gneiss being homogeneous at a scale of 28.5 m and because the mesoscopic planar fabric is not expressed by outcrop orientation. To the west, the gneiss terminates against the volcano-sedimentary sequence across a sharp contact. This contact was identified in the field as a folded thrust where the volcano-sedimentary sequence was translated eastward over the quartzo-feldspathic gneiss (Fig. 2E). This contact is distinctive in the 7-4-2 Landsat TM image where it separates the white gneissic domain in the east from a brown domain to the west (Fig. 2A). This thrust also appears in the 5/7-4/5-3/1 Landsat TM image separating a blue domain in the east from a greenish-brown domain to the west (Fig. 2B).

The north-trending volcano-sedimentary sequence occupies the area west of the quartzo-feldspathic gneiss (Fig. 2E) and is dominated by mafic schists with abundant hornblende and biotite with subordinate metasedimentary layers, including quartzite and marble, up to tens of metres wide. In the southeastern part of the volcano-sedimentary sequence, the schists are intercalated with lower grade volcanogenic agglomerate, andesite and rhyolite. The sequence has a strong north-trending, east-dipping foliation, which is steep in the west and becomes more moderate to the east. In the 7-4-2 Landsat TM image, the volcano-sedimentary sequence appears as alternating dark brown, brown and blue stripes (Fig. 2A). In the 5/7-4/5-3/1 Landsat TM image, the stripes representing the volcano-sedimentary rocks are yellowish-brown, dark brown, pink, green, blue and yellow (Fig. 2B). Locally, hornblende schist grades into discontinuous amphibolite lenses that are distinctively dark brown in the 5/7-4/5-3/1 Landsat TM image (Fig. 2B, E). A 50–100 m wide marble band is intercalated with the mafic schists and can be traced north-south for over 25 km (Fig. 2E). This marble band appears yellow in the northern part of the 5/7-4/5-3/1 Landsat TM image and pale yellowish-pink further south (Fig. 2B). In the 7-4-2 Landsat TM image, the marble band can be distinguished by its pale blue colour (Fig. 2A).

The central and southwestern parts of the Beddaho area are occupied by a syn-tectonic granodiorite. The granodiorite is deformed along sub-vertical, north-trending foliation planes, which also show sub-horizontal stretching lineation. These fabrics resulted from sinistral strike-slip shear deformation. The granodiorite body hosts the Beddaho Alteration Zone and may have provided the hydrothermal fluids responsible for clay and Fe alteration. East of the alteration zone the granodiorite appears yellowish-green, bluish-green and blue in the 5/7-4/5-3/1 Landsat TM image (Fig. 2B). West of the alteration zone, the granodioritic body is orange to yellow in colour in the 5/7-4/5-3/1 Landsat TM image (Fig. 2B). These areas appear green in the 7-4-2 Landsat TM image (Fig. 2A) and deep blue to black in the Shuttle radar image (Fig. 2C). This is due to effects of illumination and shadow associated with northwest-trending high ridges of the granodioritic body.

Two post-tectonic granitic bodies intrude the northern part of the volcano-sedimentary sequence (Fig. 2E). One lies in the extreme north and is about 1 km in diameter; this appears lime in the 5/7-4/5-3/1 Landsat TM image (Fig. 2B). The one to the south is about 4 km in diameter and is patchy yellow in the 5/7-4/5-3/1 Landsat TM image. In the 7-4-2 Landsat TM images (Fig. 2B), the northern body appears elliptical in shape with a light brown eastern half (illuminated side) and a dark brown western half (shadow side). The southern granitic body is green to brownish-green in the 7-4-2 Landsat TM image (Fig. 2A). The elliptical nature of these post-tectonic bodies is apparent in the shuttle radar image (Fig. 2C). In this image, both bodies are dark blue rounded features surrounded by brownish colour (Fig. 2C).

The Beddaho Alteration Zone is a north-trending, ~ 25 km long, 1–4 km wide zone of clay- and Fe-rich hydrothermal alteration (Fig. 2E). The alteration zone is dominantly enclosed in the syn-tectonic granodioritic body but extends north into the volcano-sedimentary sequence. The alteration affects a north-elongated roof pendant composed of sericite schist, kyanite quartzite and marble that are enclosed in the syn-tectonic granodiorite. Mineralisation is thought to be concentrated at the roof pendant because the latter provided pathways for hydrothermal fluids emanating from the syn-tectonic granodiorite (Toogood, *pers. comm.*). The contact between the granodiorite and the roof pendant rocks is gradational, as hydrothermally altered granodiorite is replaced by bleached granodiorite (Fig. 3A) with obvious loss of ferromagnesium minerals. Locally, the granodiorite/roof pendant contact is sheared

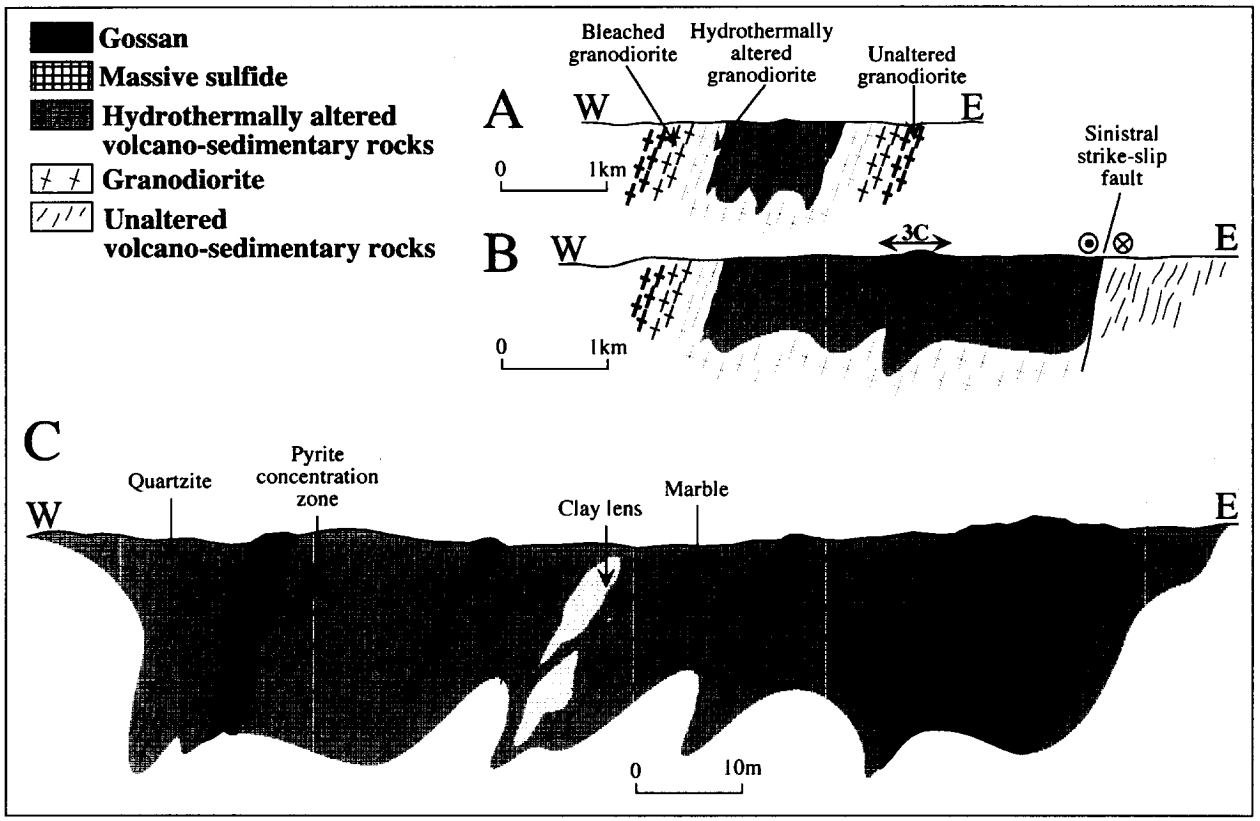

Figure 3. *Idealised geological cross-section. (A) The central part of the Beddaho Alteration Zone. (B) The southern part of the Beddaho Alteration Zone. (C) The Tebih Gossan. For the location of sections, see Fig. 2D.*

and the prominent north-trending foliation is marked by growth of amphibole and kyanite. The alteration is interpreted to postdate the emplacement of the granodiorite but predates development of the north-trending foliation and is, therefore, thought to be a result of Neoproterozoic hydrothermal activity. The kyanite might be a product of high-grade metamorphism of an originally clay-rich zone. The most common manifestation of the Fe alteration is the presence of limonite and jarosite, whereas clay alteration produced widespread sericitisation. The Fe alteration is sometimes concentrated as gossans. These gossans are dominantly massive limonite with stock work quartz veins that vary in concentration from one place to another. Euhedral pseudomorphs of limonite after pyrite crystals are common in the sericite schist. The gossans in Eritrea might have formed in the Palæogene since some of them, such as those in the Dibarwa area south of Asmara, are unconformably overlain by 30 Ma flood basalt (Drury, *pers. comm.*).

The Beddaho Alteration Zone reaches its maximum width in the south and narrows northward (Fig. 2D). It is distinctively pink in the 5/7-4/5-3/1 Landsat TM image (Fig. 2B), whereas the southern part of the alteration zone appears brownish-yellow in the 7-4-2 Landsat TM image (Fig. 2A). It is not obvious on the Chh-Lhh-Lhh/Chh image (Fig. 2C).

REMOTE SENSING ANALYSIS

The objective of the remote sensing analysis is to identify gossans within clay- and Fe-rich alteration zones using Landsat TM and SIR-C images. The Landsat TM visible and near infrared (VNIR) data were acquired in April, 1986 with Landsat 4. The SIR-C is experimental multi-frequency and multi-polarisation radar data collected in April, 1994 by the National Aeronautics and Space Administration (NASA). These were collected together with X band synthetic aperture radar (SAR) data collected by the German Aerospace Center 'Deutsches Zentrum fur Luft-und Raumfahrt' (DLR), and the Italian Space Agency 'Agenzia Spaziale Italiana' (ASI) using the space shuttle Endeavour. These data were collected in three wavelengths including L, C and X band (wavelength = 3 cm). L and C bands were collected with like-polarisations hh and vv (vertically transmitted and vertically received), cross-polarisations hv (horizontally transmitted and vertically received) and vh (vertically transmitted and horizontally received), and total power (tp). X band data were collected with polarisation vv

only. In the remote sensing analysis done in this study, X band was not used because its wavelength (3 cm) is relatively comparable to that of C band (6 cm). X band lacks polarisation hh that enhances the perceived surface roughness of the imaged object (Lewis *et al.*, 1998).

A number of gossans occur within the Beddaho Alteration Zone, the largest of which (~500 m × 500 m) occurs in the south and is named the Tebih Gossan (Figs 2E, 3 and 4). Most other gossans are too small to be unequivocally identified directly in the Landsat TM and SIR-C images that have ~30 m spatial resolution, respectively. Below is described how these data were used by the authors to locate and map alteration zones and associated gossans.

Density slicing

The density slicing technique converts the continuous grey tone of an image into a series of density intervals, each corresponding to a specific range of digital numbers (DN) (Sabins, 1997). Different density slices can be shown as separate colours and can be draped over background images. Density slicing of Landsat TM band-ratio 5/7 and 3/1 are used to create clay and Fe alteration index maps, respectively (Fig. 5A, B). Landsat TM band-ratio 5/7 effectively maps clay alteration because clay minerals such as sericite have reflectance maxima within band 5 similar to most minerals (reflected IR; wavelength = 1.55–1.75 μm) and reflectance minima within band 7 (reflected IR; wavelength = 2.08–2.35 μm) (Hunt and Ashley, 1979). Similarly, Landsat TM band-ratio 3/1 is effective in mapping Fe alteration because Fe minerals such as limonite and jarosite have reflectance maxima within band 3 (visible red; wavelength = 0.63–0.69 μm) and reflectance minima within band 1 (visible blue; wavelength = 0.45–0.52 μm) (Hunt *et al.*, 1971). Hence, 5/7 and 3/1 Landsat TM band-ratios increase the difference between the DN values of clay and Fe alteration zones, respectively, and those of unaltered rocks. This leads to better discrimination between hydrothermally altered and unaltered zones (Fig. 5A, B). These index maps show excellent correlation with field observation by the authors as well as other investigators (Toogood, *pers. comm.*). Density slicing was also successfully used to map clay- and Fe-rich alteration zones along the Neoproterozoic Allaqi Suture in southern Egypt (Ramadan *et al.*, *in press*).

The clay- and Fe-rich alteration index maps reveal the Tebih Gossan as a horseshoe-shaped structure with maximum Fe concentration (Fig. 5C) and lacking clay alteration (Fig. 5D). Comparing clay and Fe alteration index maps with the 5/7-4/5-3/1 Landsat TM (Fig. 5E) and shuttle radar (Fig. 5G) images led to the identification of the Tebih Gossan in these images. In the 5/7-4/5-3/1 Landsat TM image, the Fe-rich areas such as those occupied by the Tebih Gossan appear dark bluish, areas dominated by clay alteration appear red, and when both mineral species are present the area appears magenta in colour (Fig. 5E). The Tebih Gossan is characteristically red in the shuttle radar image (Fig. 5G). The blue colour of the Tebih Gossan in the 5/7-4/5-3/1 Landsat TM image is due to the fact that band-ratio 3/1 is assigned to blue in the RGB colour overlay (Fig. 2D). The red appearance of the Tebih Gossan in the shuttle radar image might be due to enhancement of back-scattering of the shorter wavelength (6 cm) C band by the gossan's rough surfaces. This might also be partially due to the distinctive dielectric property of the Fe-rich minerals forming the gossans (Lewis *et al.*, 1998). In the RGB colour overlay the C-band is assigned to red. It should be stressed here that the shuttle radar image alone might not be useful in finding and mapping gossans. The authors were able to find the Tebih Gossan in this image because it was compared with the 5/7-4/5-3/1 Landsat TM image.

Supervised classification

This technique involves selecting a pixel or a cluster of pixels with known geological meaning as a training site and using these to locate regions with similar spectral characteristics. Choice of the training site is done in the 5/7-4/5-3/1 Landsat TM image and the shuttle radar image. These images are chosen because they best identify the gossans. The Landsat TM training area involves 32 pixels that overlap with the Tebih Gossan and have similar DN values. Similarly, 17 pixels were used for the training site in the SIR-C image. The complete Tebih Gossan occupies an area covered by ~200 pixels (Fig. 5C, D). Parallelepiped supervised classification based on bands 1, 2, 3, 4, 5 and 7 of the Landsat TM data and bands Lhh, Lhv, Chh and Chv of the SIR-C data was conducted to outline areas with reflectance spectra and radar back-scattering similar to those of pixels representing the Tebih Gossan (Fig. 5F, H). Lhh, Lhv, Chh, and Chv SIR-C bands were used to evaluate the multi-frequency and multi-polarisation capability of the radar data in the supervised classification. SIR-C data over the Beddaho Alteration Zone also contain Ltp and Ctp but were not used in the supervised classification because these lack polarisation. Polarisation (among other system-related factors) controls the perceived surface roughness of the imaged materials (Lewis *et al.*, 1998). To ensure that areas similar in their reflectance spectra and back-scattering to the Tebih Gossan would be identified, a maximum standard deviation of 1 was chosen. These results show significant correlation

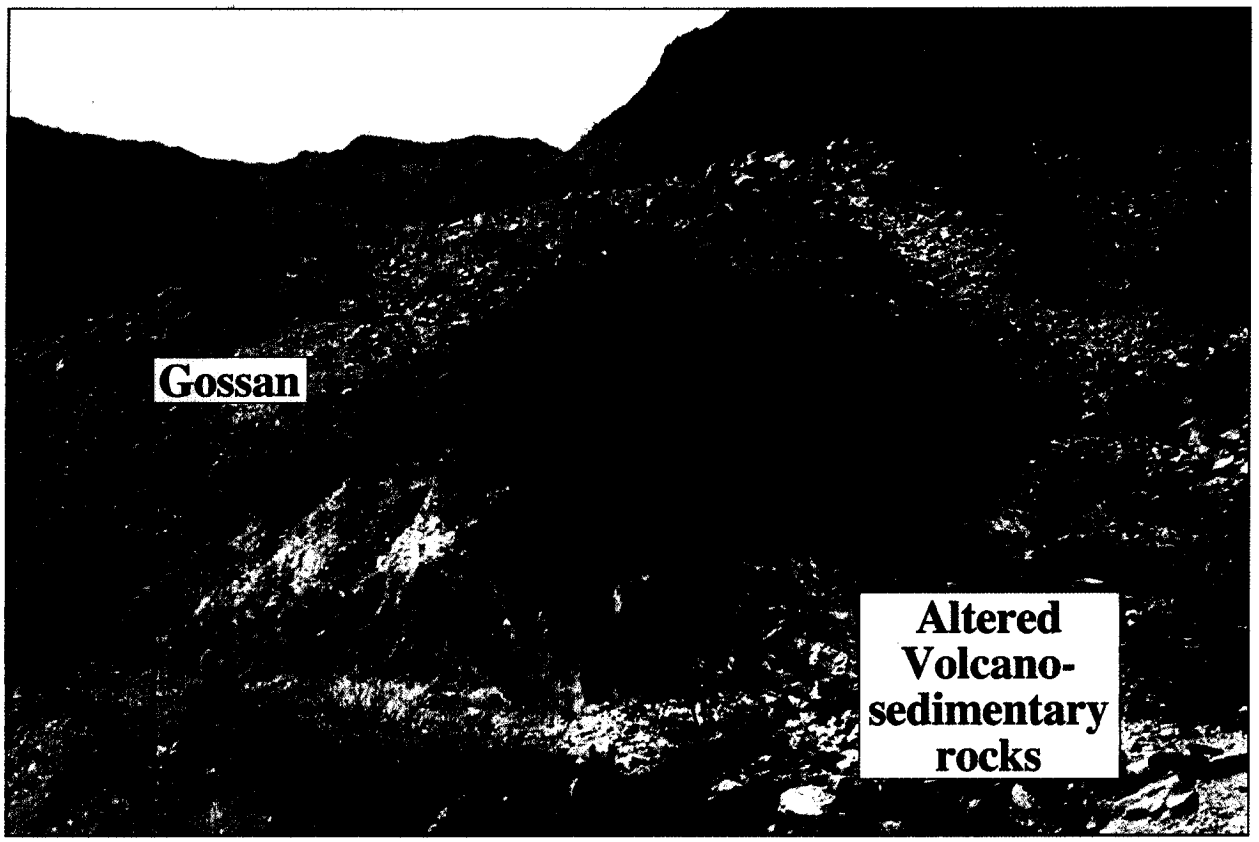

Figure 4. *The Tebih Gossan.*

between supervised classifications based on Landsat TM and SIR-C data sets (Fig. 5F, H, I). Scattering of red dots in the supervised classification 3/1 Landsat TM and the Chh SIR-C images might be due to the presence of smaller (few pixels) gossan-like material along the Beddaho Alteration Zone. This might be due to dispersion of debris because of high relief.

DISCUSSION

Resolution and coverage considerations

Landsat TM data have been used to map alteration zones because of their characteristic spectral properties (Abrams *et al.*, 1983; Buckingham and Sommer, 1983; Goetz *et al.*, 1983; Drury and Hunt, 1988; Kaufmann, 1988; Amos and Greenbaum, 1989; Kaufmann and Kruck, 1989; Frei and Jutz, 1989; Rockwell, 1989; Kruse, 1989; Fraser, 1991; Loughlin, 1991; Filho *et al.*, 1996; Filho and Vitorello, 1997; van der Meer, 1997; Ruiz-Armenta and Prol-Ledesma, 1998). Landsat TM data have not been used before specifically to identify gossans within a wider alteration zone. This may be partly because the 28.5 m spatial resolution of the Landsat TM data is too coarse to be used in direct identification of the majority of gossans that are only a few tens of metres across.

The density slicing technique proved useful in overcoming the spatial resolution disadvantage of the Landsat TM data in mapping few pixel gossans in that:

i) the density slicing technique produces clay and Fe alteration index maps, which can be used to identify alteration zones that sometimes (as in the case of the Arabian-Nubian Shield) contain gossans; and

ii) comparing clay and Fe alteration index maps led to the identification of gossans.

Iron-rich gossans usually show high DN values in the Fe alteration index maps. This is different from the gossan appearance in the clay alteration index map where they have low DN values.

Using VNIR remote sensing data with spatial resolution better than Landsat TM data may be useful for identifying gossans in the Arabian-Nubian Shield and other arid regions. Moreover, merging Landsat TM and Satellite Probatoire pour l'Observation de la Terre (SPOT) data has been used to map lithological details (Yesou *et al.*, 1993). However, Landsat TM data is important in exploring for Au-bearing massive sulphides in these regions because:

i) Landsat TM images allow large areas to be examined inexpensively (a Landsat TM scene is 185 × 175 km).

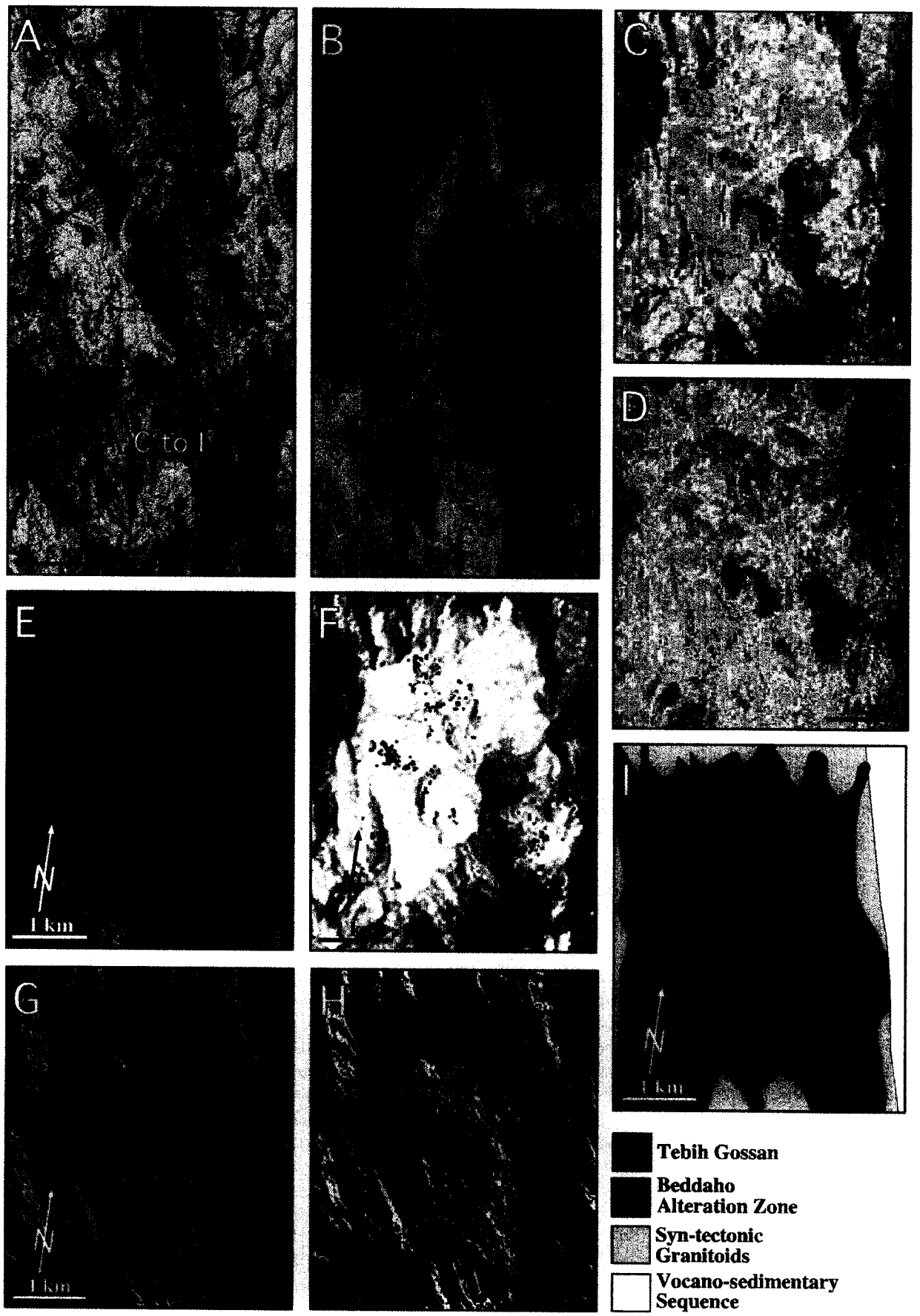
A
B
C
D
E
F
G
H
I
A to I
N
1 km
N
1 km
N
1 km
Tebih Gossan
Beddaho Alteration Zone
Syn-tectonic Granitoids
Vocano-sedimentary Sequence

ii) Landsat TM data have better spectral resolution and range than high spatial resolution VNIR data such as SPOT. The multi-spectral SPOT XS data have two bands in the visible and one in the near infrared regions of the electromagnetic spectrum, comparable to Landsat TM bands 2, 3 and 4. SPOT XS data lack bands that would allow mapping clay alteration minerals.

iii) Landsat TM data are relatively inexpensive and, therefore, are affordable by developing countries in arid regions.

Use of VNIR remote sensing data with better spatial and spectral resolution promises to enable better mapping of alteration zones, and hyperspectral imaging promises to become increasingly important for mineral exploration in the developing countries of north Africa and other arid regions. As an example, the airborne visible and infrared imaging spectrometer (AVIRIS) optical system collects VNIR data with 224 bands with a spectral resolution of 10 nm and spectral range between 400 to 2500 nm, with a nominal spatial resolution of 20 m. These data have been extensively used for mapping Fe and clay minerals of alteration zones associated with the Cuprite mining district in Nevada (Taranik and Kruse, 1989; Clark *et al.*, 1990, 1991, 1992, 1993; King, 1995a, b). Recent low-altitude flights collected data with 3–2 m spatial resolution (Swayze *et al.*, 1999). AVIRIS data, although they are spatially and spectrally superior to orbital VNIR data, are experimental and cover small (an AVIRIS scene is 7.5 × 7.5 km), selected areas. This makes AVIRIS data less useful compared to Landsat TM data in mineral exploration in poorly mapped regions where vast areas are to be considered.

Application of SIR-C data to mineral exploration

Radar imaging techniques have not been used for direct detection of mineral deposits, although some SAR data have been integrated with Landsat TM and geophysical data to understand lithological and structural controls on ore bodies (Rheault *et al.*, 1989; Harris, 1989; Rowan and Bowers, 1995). Radar back-scattering is a function of surface roughness together with other environment- and system-related factors (Lewis *et al.*, 1998). Hence, radar can be used to map surficial deposits such as alluvial fans, lava flows and glacial debris (Singhroy *et al.*, 1989; Farr and Chadwick, 1996; Weeks *et al.*, 1996; Zebker *et al.*, 1996). The work presented here encourages further examination of the potential of using orbital imaging radar data such as SIR-C to explore for minerals. SIR-C data are experimental and cover selected parts of the earth surface. However, commercial orbital radar data such as RADARSAT are available. These data, however, contain a single radar band and have one polarisation (Chh in the case of RADARSAT) unlike SIR-C data, which are multi-frequency and multi-polarisation. Exploration strategies that couple imaging radar with VNIR data sets would be advantageous in that more than one characteristic, such as reflectance spectra and surface roughness, can be used in the search for gossans, improving the certainty of the search. This technique might lead to the discovery of new massive sulphide deposits in the Arabian-Nubian Shield and other arid regions. This is because:

i) Some mineral deposits outcrop with distinctive roughness compared to the surrounding rocks. Massive sulphide deposits capped with gossans are likely to be imaged with radar because of the characteristic weathering pattern of these deposits which translates into surface roughness distinctive enough to enhance radar back-scattering. This effect is likely to be seen best in areas of subdued relief.

ii) Radar is often better than VNIR images for mapping regional structures, hence can be helpful in understanding structural controls on mineralisation.

Complications due to laterites

Humid conditions in the southern part of the Arabian-Nubian Shield led to the development of Fe-rich lateritic soils during Early Tertiary times. These palæosoils are overlain by Tertiary flood basalts in parts of Eritrea, Ethiopia, Saudi Arabia and Yemen and have been exhumed where the basalts are removed by erosion. Isolated lateritic patches extend as far north as 15°20'N (Fig. 1)(Drury *et al.*, 1994). These laterites contain ferricrete horizons which are superficially similar to gossans and which have complicated mineral exploration efforts in Saudi Arabia (Ryall and Taylor, 1981). Lateritic Fe-rich and clay-rich components could be difficult to distinguish from true gossans. It is not expected that this is a problem for the Beddaho example because:

Figure 5. *(A) Clay alteration index map of the Beddaho Alteration Zone draped over a 5/7 Landsat TM image. (B) Iron alteration index map of the Beddaho Alteration Zone draped over a 3/1 Landsat TM image. In both alteration index maps the DNs of the density slices are calculated to represent the top ~5% (red), ~10% (orange) and ~15% (yellow). This corresponds to DNs of 255-242, 241-228 and 227-214 in the clay alteration index map and DNs of 255-242, 241-228 and 227-214 in the Fe alteration index map. (C–E) 5/7-4/5-3/1 Landsat TM images for the Tebih Gossan. (F) Results of Parallelepiped supervised classification (in red) using the Tebih Gossan as a training site, based on bands 1, 2, 3, 4, 5 and 7 of the Landsat TM data. The background is a 5/7 Landsat TM image. (G) Chh-Lhh-Lhh/Chh SIR-C image of the Tebih Gossan. (H) Results of Parallelepiped supervised classification (in red) using the Tebih Gossan as a training site, based on bands Lhh, Lhv, Chh and Chv of the SIR-C/X-SAR data. The background is a Lhh SIR-C image. (I) Geological map.*

i) Beddaho lies further north than the most northerly laterite mapped in Eritrea (Drury *et al.*, 1994); and

ii) in contrast to laterites that define the pre-mid Tertiary erosion surface, the Beddaho Alteration Zone expresses basement structural control.

There is no evidence for a nearby exhumed surface or palæosoil, so the Fe and clay alteration zones are not likely to have resulted from deep weathering of ancient erosion surfaces.

Although the present study has not been compromised by complications due to the occurrence of laterites, it can be anticipated that these may make mineral exploration further south more difficult.

CONCLUSIONS

Clay and Fe alteration index maps produced by density slicing of the Landsat TM band-ratio 5/7 and 3/1, respectively, are useful in mapping zones of alteration associated with massive sulphide mineralisation. Clay and Fe alteration index maps are also useful in identifying the few tens of metres across gossans despite the 28.5 m spatial resolution of Landsat TM data. Gossans show as areas with low DN values in the clay alteration index map and are indicated by high DN values in the Fe alteration index map. The Tebih Gossan is identifiable in 5/7-4/5-3/1 Landsat TM images and shuttle radar images. Using both Landsat TM and SIR-C data is advantageous in that more than one feature (reflectance spectra and surface roughness) may be used to search for gossans during supervised classification. This, in turn, increases the likelihood of success of the technique in finding new gossan occurrences in the Arabian-Nubian Shield and other arid regions.

ACKNOWLEDGEMENTS

The authors would like to thank the Department of Mines, Eritrea, and Phelps Dodge, South Africa, for their help during the field phase of this work. They would also like to thank D. Toogood for his field assistance and discussion. This work was supported by a National Aeronautics and Space Administration (NASA) contract administered through the Jet Propulsion Laboratory (JPL). Thanked are S. Drury and L. Chevallier for detailed reviews of the manuscript.

Editorial handling - R.J. Thomas

REFERENCES

Abdelsalam, M.G., 1994. The Oko shear zone: post-accretionary deformations in the Arabian-Nubian Shield. Journal Geological Society, London 151, 767–776.

Abdelsalam, M.G., Robinson, C., El-Baz, F., Stern, R.J., 2000. Application of orbital imaging radar in geology studies in arid regions: the Saharan testimony. Journal Photogrammetric Engineering Remote Sensing 66, 717–726.

Abdelsalam, M.G., Stern, R.J., 1996a. Sutures and Shear Zones in the Arabian-Nubian Shield. Journal African Earth Sciences 23, 289–310.

Abdelsalam, M.G., Stern, R.J., 1996b. Mapping Precambrian structures in the Sahara Desert with SIR-C/X-SAR Radar: The Neoproterozoic Keraf Suture, NE Sudan. Journal Geophysical Research, 23,063–23,076.

Abrams, M.J., Brown, D., Lepley, L., Sadowski, R., 1983. Remote Sensing for Porphyry Copper Deposits in southern Arizona. Economic Geology 78, 591–604.

Al-Shanti, A.M.S., Roobol, M.J., 1979. Some thoughts on Metallogenesis and Evolution of the Arabian-Nubian Shield. In: Al-Shanti, A.M.S. (Ed.), Evolution and Mineralization of the Arabian-Nubian Shield. Pergammon Press, New York, pp. 87–96.

Amos, B.J., Greenbaum, D., 1989. Alteration detection using TM imagery, the effect supergene weathering in an arid climate. International Journal Remote Sensing 10, 515–527.

Aye, F., Cheze, Y., El-Hindi, M., 1985. Discovery of a major massive sulfide province in northeastern Sudan. In: Proceedings Conference on Prospecting in Areas of Deseart Terrains, Rabat, Morocco, pp. 43–48.

Bakheit, A.K., Matheis, G., 1993. Gold-productive volcanogenic sulphide mineralization in the Ariab Belt, Red Sea Hills, Sudan: Evidence for Late Proterozoic seafloor hydrothermal systems. In: Thorweiehe U., Schandelmeier, H. (Eds.), Geoscientific Reseasrch in Northeast Africa. Balkema, Roterdam, pp. 533–540.

Beyth, M., Stern, R.J., Matthews, A., 1997. Significance of high-grade metasediments from the Neoproterozoic basement of Eritrea. Precambrian Research 86, 45–58.

Buckingham, W.F., Sommer, S.E., 1983. Mineralogical Characterization of rock surfaces formed by Hydrothermal Alteration and Weathering - Application to Remote Sensing. Economic Geology 78, 664–674.

Clark, R.N., Gallagher, A.J., Swayze, G.A., 1990. Material Absorption Band Depth Mapping of Imaging Spectrometer Data Using a Complete Band Shape Least-Squares Fit with Library Reference Spectra. Jet Propulsion Laboratory Publication 90–54, 176–186.

Clark, R.N., Swayze, G.A., Gallagher, A., 1992. Mapping the Mineralogy and Lithology of Canyonlands, Utah with Imaging Spectrometer Data and the Multiple Spectral Feature Mapping Algorithm. Jet Propulsion Laboratory Publication 92–14, 11–13.

Clark, R.N., Swayze, G.A., Gallagher, A., 1993. Mapping Minerals with Imaging Spectroscopy. US Geological Survey Office of Mineral Resources Bulletin 2039, 141–150.

Clark, R.N., Swayze, G.A., Gallagher, A., Gorelick, N., Kruse, F., 1991. Mapping with Imaging Spectrometer Data Using the Complete Band Shape Least-Squares Algorithm Simultaneously Fit to Multiple Spectral Features from Multiple Materials. Jet Propulsion Laboratory Publication 91–28, 2–3.

Cottard, F., Braux, C., Cortial, P., Deschamps, Y., El-Samani, Y., 1986. Gold and massive sulphide deposits of Ariab area, development and exploration results. GRAS/BRGM Report 85 SDN 011, 55p.

De Souza Filho, C.R., Drury, S.A., 1998. A Neoproterozoic supra-subduction terrane in northern Eritrea, NE Africa. Journal Geological Society London 155, 551–566.

Drury, S.A., Berhe, S.M., 1993. Accretion tectonics in northern Eritrea revealed by remotely sensed imagery. Geological Magazine 130, 177–190.

Drury, S.A., de Souza Filho, C.R., 1999. Neoproterozoic terrane assemblages in Eritrea: review and prospects. Journal African Earth Sciences 27, 331–348.

Drury, S.A., Hunt, G.A., 1988. Remote sensing of laterized archaean greenstone terrain: Marshall Pool area, northern Yilgarn block, western Australia. Journal Photo-grammetric Engineering Remote Sensing 54, 1717–1725.

Drury, S.A., Kelley, S.P., Berhe, S.M., Collier, R.E.L., Abraha, M., 1994. Structures related to Red Sea evolution in northern Eritrea. Tectonics 136, 1371–1380.

Farr, T.G., Chadwick, O.A., 1996. Geomorphic processes and remote sensing signatures of alluvial fans in the Kun Lun Mountains, China. Journal Geophysical Research 101, 23,091–23,100.

Filho, R.A., Vitorello, I., 1997. Remote sensing and field data integration in the definition of hydrothermally altered areas in vegetated terrain, central Brazil. International Journal Remote Sensing 18, 1835–1842.

Filho, R.A., Vitorello, I., Correia, V.R.M., 1996. Use of Landsat Thematic Mapper Imagery as mineral prospecting tool in the tin province of Goias, Brazil. Geocarto International 11, 61–69.

Fraser, J., 1991. Discrimination and identification of ferric oxides using satellite Thematic Mapper data; a Newman case study. International Journal Remote Sensing 12, 635–641.

Frei, M., Jutz, L., 1989. Use of Thematic Mapper data for the detection of gold bearing formations in the Eastern Desert of Egypt. In: Proceedings 7th Thematic Conference on Remote Sensing in Exploration Geology, Calgary, Canada, pp. 1157–1172.

Goetz, A.F.H., Rock, B.N., Rowan, L.C., 1983. Remote sensing for exploration: an overview. Economic Geology 78, 573–590.

Goldsmith, R., Kouther, J.H., 1971. Geology of the Mahd adh Dhahab - Umm ad Damar area, Kingdom of Saudi Arabia. Direcorate General of Mineral Resources, Kingdom Saudi Arabia Mineral Resources Bulletin 6, 20p.

Harris, J., 1989. Data integration for gold exploration in eastern Nova Scotia using a GIS. In: Proceedings 7th Thematic Conference on Remote Sensing in Exploration Geology, Calgary, Canada, pp. 233–250.

Hume, W.F., 1937. Geology of Egypt, Vol. II The Fundamental Pre-Cambrian Rocks of Egypt and the Sudan, their Distribution, Age and Character, Part III. The Minerals of Economic Value. Government Press, Cairo, 300p.

Hunt, G.R., Ashley, R.P., 1979. Spectra of altered rocks in the visible and near infrared. Economic Geology 74, 1613–1629.

Hunt, G.R., Salisbury, J.W., Lenhoff, C.J., 1971. Visible and near-infrared spectra of minerals and rocks: III. Oxides and hydroxides. Modern Geology 2, 195–205.

Johnson, P.R., 1994. The Nakasib suture: a compilation of recent information about a Sudanese fold and thrust belt, and implications for the age, structure and mineralization of the Bir Umq suture, Kingdom of Saudi Arabia. USGS Open-File Report USGS-OF-94-6, 44p.

Kaufmann, H., 1988. Exploration along the Aqaba-Levant structure by use of TM data - concepts, processing and results. International Journal Remote Sensing 9, 1639–1658.

Kaufmann, H., Kruck, W., 1989. Mineral exploration in the Yemen Arab Republic by use of TM-data (Preliminary results). In: Proceedings 7th Thematic Conference on Remote Sensing in Exploration Geology, Calgary, Canada, pp. 1223–1227.

Kearey, P., 1993. The Encyclopedia of the Solid Earth Sciences. Blackwell, Oxford, 713p.

Key, R.M., Charsley, T.J., Hackman, T.J., Wilkinson, A.F., Rundle, C.C., 1989. Superimposed upper Proterozoic collision controlled orogenies in the Mozambique Orogenic belt of Kenya. Precambrian Research 44, 197–225.

King, T.V.V., Clark, R.N., Ager, C., Swayze, G.A., 1995a. Remote mineral mapping using AVIRIS data at Summitville, Colorado and the adjacent San Juan Mountains. Colorado Geological Survey Special Publication 38, 59–63.

King, T.V.V., Clark, R.N., Ager, C., Swayze, G.A., 1995b. Remote mineral mapping using AVIRIS data at Summitville, Colorado and the adjacent San Juan Mountains. Jet Propulsion Laboratory Publication 95–1, 113–116.

Kröner, A., Linnebacher, P., Stern, R.J., Reischmann, T., Manton, W., Hussein, I.M., 1991. Evolution of Pan-African island arc assemblages in the southern Red Sea Hills, Sudan, and in southwestern Arabia as exemplified by geochemistry and geochronology. Precambrian Research 53, 99–118.

Kruse, F.A., 1989. Spectral mapping with Landsat Thematic Mapper and imaging spectroscopy for precious metals exploration. In: Proceedings 7th Thematic Conference on Remote Sensing in Exploration Geology, Calgary, Canada, pp. 15–28.

Lewis, A.J., Henderson, F.M., Holcomb, D.W., 1998. Radar fundamentals: the Geoscience prospective. In: Henderson, F.M., Lewis, A.J. (Eds.), Principals and Applications of Imaging Radar. John Wiley and Sons, New York, pp. 131–181.

Loughlin, W.P., 1991. Principal component analysis for alteration mapping. Journal Photogrammetric Engineering Remote Sensing 57, 1163–1169.

Miller, M.M., Dixon, T.H., 1992. Late Proterozoic evolution of the N part of the Hamisana zone, northeast Sudan: constraints on Pan-African accretionary tectonics. Journal Geological Society London 149, 743–750.

Mosely, P.N., 1993. Geological evolution of the late Proterozoic 'Mozambique Belt' of Kenya. Tectonophysics 221, 223–250.

Ramadan, T.M., Abdelsalam, M.G., Stern, R.J. In press. Mapping gold-bearing massive sulfide deposits in the Neoproterozoic Allaqi suture, SE Egypt with Landsat TM and SIR-C/X-SAR images. Journal Photogrammetric Engineering Remote Sensing.

Rheault, M., Simard, R., Garneau, C., Slaney, V.R., 1989. SAR-Landsat TM - Geophysical data integration utility of value-added products in geological exploration. In: Proceedings 7th Thematic Conference on Remote Sensing in Exploration Geology, Calgary, Canada, pp. 549–559.

Rockwell, B.W., 1989. Hydrothermal alteration mapping in spectral ratio feature space using TM reflectance data: Aurora Mining District, Mineral County, Nevada. In: Proceedings 7th Thematic Conference on Remote Sensing in Exploration Geology, Calgary, Canada, pp. 1189–1205.

Rowan, L.C., Bowers, T.L., 1995. Analysis of linear features mapped in Landsat Thematic Mapper and side -looking airborne radar images of the Reno 1° by 2° quadrangle, Nevada and California: implication for mineral resource studies. Journal Photogrammetric Engineering Remote Sensing 61, 749–759.

Ruiz-Armenta, J.R., Prol-Ledesma, R.M., 1998. Techniques for enhancing the spectral response of hydrothermal alteration minerals in Thematic Mapper images of central Mexico. International Journal Remote Sensing 19, 1981–2000.

Ryall, W.R., Taylor, G.F., 1981. Gossan evaluation manual: For use in the Kingdom of Saudi Arabia. Saudi Arabian Deputy Ministry for Mineral Resources Technical Record RF-TR-01-3, 146p.

Sabins, F.F., 1997. Remote sensing principles and interpretation. W.H. Freeman and Company, New York, 494p.

Sato, T., 1974. Distribution and geological setting of the Kuroko deposits. In: Ishihara, S. (Ed.), Geology of Kuroko Deposits. The Society Mining Geologist Japan Special Issue 6, pp. 1–9.

Shackleton, R.M., 1986. Precambrian collision tectonics in Africa. In: Coward, M.P., Ries, A.C. (Eds.), Collision Tectonics. Geological Society London, Special Publication 19, pp. 329–349.

Singhroy, V.H., Kenny, F.M., Barnett, P.J., 1989. Radar imagery for Quaternary geological mapping in glaciated terrains. In: Proceedings 7th Thematic Conference on Remote Sensing in Exploration Geology, Calgary, Canada, pp. 591–600.

Stern, R.J., 1994. Arc Assembly and continental collision in the Neoproterozoic East African Orogen: Implications for the consolidation of Gondwanaland. Annual Reviews Earth Planetary Science 22, 319–351.

Stoeser, D.B., Camp, E., 1985. Pan-African microplate accretion of the Arabian Shield. Geological Society America Bulletin 96, 817–826.

Swayze, G.A., Clark, R.N., Alex, F.H., Goetz, K., Livo, K., Sutley, S.S., 1999. AVIRIS 1998 Low Altitude Versus High Altitude Comparison Over Cuprite, Nevada, Sutley, http://www.speclab.cr.usgs.gov/cuprite98-low/cuplow+high.html

Taranik, D.L., Kruse, F.A., 1989. Iron mineral reflectance in Geophysical and Environmental Research Imaging Spectrometer (GERIS) data. In: Proceedings 7th Thematic Conference on Remote Sensing in Exploration Geology, Calgary, Canada, pp. 445–459.

Teklay, M., 1997. Petrology, geochemistry, and geochronology of Neoproterozoic magmatic arc rocks from Eritrea: implication for crustal evolution in the southern Nubian Shield. Department of Mines, Eritrea, Memoir 1, 125p.

Van der Meer, F., 1997. Mineral mapping and Landsat Thematic Mapper image classification using spectral unmixing. Geocarto International 12, 27–40.

Weeks, R.J., Smith, M., Pak, K., Li, W., Gillespie, A., Gustafson, B., 1996. Surface roughness, radar backscatter and visible and near-infared reflectance in Death Valley, California. Journal Geophysical Research 101, 23,077–23,090.

Wipfler, E.L., 1994. Geochemische, strukturelle und erzmikroskopische Untersuchungen zur Lagerstattenentwicklung des westlichen Ariab Nakasib Belt, Red Sea Provinz, NE Sudan. Berliner Geowissenschaften Abhandlungen 166, 206p.

Yesou, H., Besnus, Y., Rolet, J., 1993. Extraction of spectral information from Landsat TM data and merger with SPOT panchromatic imagery - a contribution to the study of geological structures. Journal Photogrammetric Remote Sensing 48, 23–36.

Zebker, H.A., Rosen, P., Hensley, S., Mouginis-Mark, P.J., 1996. Analysis of active lava flows on Kilauea volcano, Hawaii, using SIR-C radar correlation measurements. Geology 24, 495–498.